JCTC Journal of Chemical Theory and Computation

Article

pubs.acs.org/JCTC

On the Sensitivity of Peptide Nucleic Acid Duplex Formation and Crystal Dissolution to a Variation of Force-Field Parameters

Stephan J. Bachmann,[†] Zhixiong Lin,[†] Thorsten Stafforst,[‡,∥] Wilfred F. van Gunsteren,[†] and Jožica Dolenc*[,†,§]

[†]Laboratory of Physical Chemistry, ETH Zürich, CH-8093 Zürich, Switzerland

[‡]Laboratory of Organic Chemistry, ETH Zürich, CH-8093 Zürich, Switzerland

[§]Faculty of Chemistry and Chemical Technology, University of Ljubljana, 1000 Ljubljana, Slovenia

Supporting Information

ABSTRACT: The technique of one-step perturbation to explore the relation between particular force-field parameters on the one hand and particular properties of a biomolecular system on the other hand from one or a few molecular dynamics simulations is applied to investigate the dependence of the free enthalpy of dimer formation and of crystal dissolution of a self-complementary fragment (H−CGTACG−NH_2) of peptide nucleic acid, PNA, a mimic of DNA. The simulations show that PNA dimer formation in aqueous solution is favored by a decrease in the base charges with respect to values of the GROMOS 45A4 force field, while it is disfavored by a decrease in the backbone charges. In contrast, crystal dissolution of the PNA dimer is favored by a decrease in base charges, while a variation of backbone charges has a minor effect on this free enthalpy change. These opposite effects in a crystalline versus aqueous solution environment can be understood from the different water contents for these systems and have consequences for biomolecular force-field development.

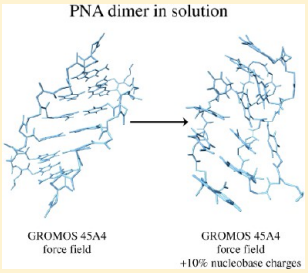

1. INTRODUCTION

After the first molecular dynamics (MD) simulations of liquids in the 1960s, this technique to investigate the properties of complex molecular systems in the condensed phase was applied to biomolecules such as proteins in the 1970s, to nucleic acids in the 1980s, and to sugars and lipids in the 1990s. Of these four basic types of biomolecules, the reliable simulation of the structural properties of nucleic acids in the form of DNA and RNA turned out to be problematic because of the abundance of negatively charged phosphate groups in these molecules and the long-range character of the Coulomb interaction.[1−4] DNA structure turned out to be sensitive to the way in which long-range Coulomb interactions were modeled, e.g., through a continuum reaction-field force or as an infinite, periodic, lattice sum,[5,6] and to the presence of counterions.[7−9] Compared to the abundance of structural data for proteins derived from experiments, there is not much high-resolution data on DNA to test the force field and computational procedures used in MD simulations of DNA. X-ray crystallographic data on DNA duplexes are only available for short nucleotide sequences and are of medium resolution. NMR data are generally insufficient in number to unambiguously determine the dominant structure of DNA in aqueous solution.

In the absence of the phosphate groups in the polynucleotide backbone of DNA, calculation of the properties, in particular energies and free energies of DNA, would be feasible because of the absence of fully charged moieties. Such an electrostatically neutral analogue of DNA is peptide nucleic acid (PNA),[10−12] first described by Nielsen et al.[13] in 1991. It is a mimic of DNA in which the deoxyribose phosphate is replaced by an N-(2-aminoethyl)glycine unit (Figure 1). As in DNA, the nucleobases adenine (A), cytosine (C), guanine (G), and thymine (T) can

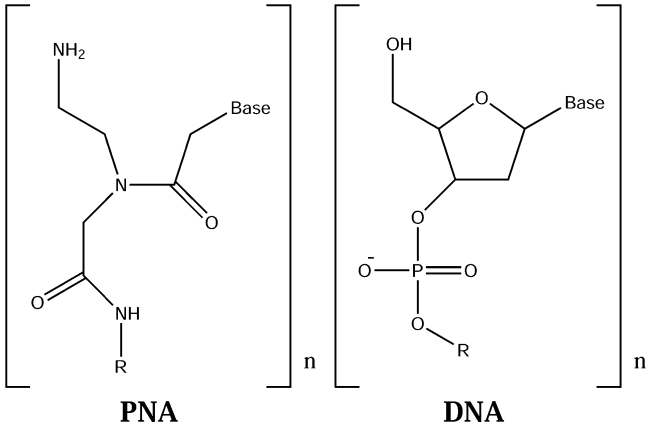

Figure 1. DNA and PNA backbones.

form A−T and G−C base pairs by forming Watson−Crick hydrogen bonds[14] between complementary hydrogen-bonding acceptor and donor sites of the nucleobases. This property has motivated several experimental[15−17] and theoretical[18−20] studies of PNA with an eye to its use as diagnostic or drug molecule. PNA might be a potential antisense or antigene drug[12] because it

Received: July 24, 2013
Published: November 13, 2013

can bind strongly and with a high sequence discrimination to complementary oligomers of DNA, RNA, or another PNA. In general, the thermal stabilities (T_m) of duplexes for identical sequences are in decreasing order: PNA−PNA > PNA−RNA > PNA−DNA > RNA−DNA > DNA−DNA.[21] PNA is also an ideal candidate for DNA force-field development because of its lack of negative charges on the backbone while having the same bases as DNA.

The goal of the present work is to investigate through free energy calculations which force-field parameters influence the stability of a PNA dimer. The changing free enthalpy of PNA dimer formation upon variation of particular force-field parameters or upon variation of its environment is calculated with the method of one-step perturbation.[22] This method is less expensive than the method of thermodynamic integration (TI) but also less precise. Its precision has been evaluated by comparison to TI results for solvation of small molecules,[22−24] for changes of force-field parameters of α-peptides[25] and β-peptides,[26] and for protein−ligand binding.[27,28] The one-step prediction of the change of folding free enthalpy upon modification of side chains has been evaluated by comparison of this quantity as obtained from counting folded versus unfolded configurations in standard MD simulations of α-peptides[29] and β-peptides.[26] Here, the reliability of the one-step perturbation results is checked by performing backward perturbations for particular combinations of parameter values.[30] Its advantage is that it allows testing of many force-field parameter value combinations and their influence on the stability of a PNA dimer from a single simulation.

Nine molecular dynamics (MD) simulations of a short PNA strand with sequence H−CGTACG−NH_2[31] have been performed (Table 1): four of the monomers (M) in solution, four of the dimers (D) in solution, and one of 24 dimers in a crystal unit cell (C). The simulations in solution were each performed without (F) and with (R) position restraints on some backbone atoms of the PNA molecules and using the GROMOS 45A4 force field without or with 10% increased partial charges on the atoms of the bases (P). Figure 2 shows the free enthalpy differences $\Delta G_{BA} = G_B - G_A$ between pairs of simulated systems (horizontal arrows) and the free enthalpy differences $\Delta G^{pert\ ref} = G^{pert} - G^{ref}$ between the systems simulated with the GROMOS 45A4 force field (ref) and a perturbation (pert) of some of its parameters (vertical rows) that can be calculated using one-step perturbation. The perturbation of +10% of the base charges was used in four simulations for backward perturbation.

Table 1. Overview of Simulations Performed

simulation name	molecule	environment	position restrained	base charges change	simulation period [ns]
DF	dimer	solution	no	no	25.5
DR	dimer	solution	yes	no	10.5
PDF	dimer	solution	no	+10%	25.5
PDR	dimer	solution	yes	+10%	10.5
MF	monomer	solution	no	no	25.5
MR	monomer	solution	yes	no	10.5
PMF	monomer	solution	no	+10%	25.5
PMR	monomer	solution	yes	+10%	10.5
DC	24 dimers	crystal	no	no	10.5

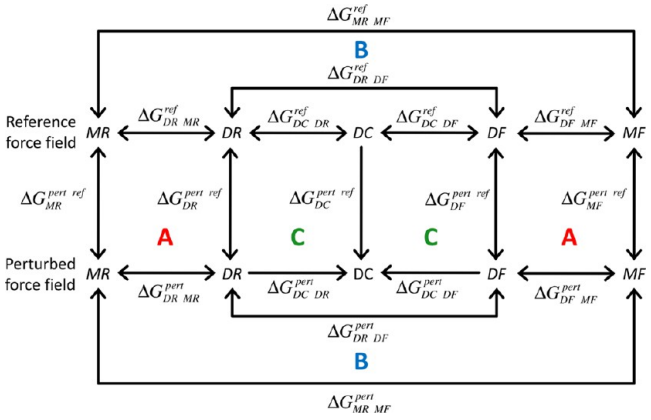

Figure 2. Names of the different systems simulated (Table 1) and free enthalpy differences ΔG that can be obtained by one-step perturbation for changes of the system (horizontal arrows, lower indices) or changes in force-field parameters (vertical arrows, upper indices). Systems and force-field parameters listed in Table 1 have names in italics. Thermodynamic cycles that are used to calculate the influence of the force-field parameters on the stability of the PNA dimer (cycles A), on position restraining on the backbone atoms of PNA (cycles B), and on changing the environment between crystal and aqueous solution (cycles C) are shown.

2. METHODS

The simulations of the self-complementary PNA fragment (H−CGTACG−NH_2) have been carried out using the GROMOS[32,33] biomolecular simulation package and the GROMOS force field 45A4.[34,35] In this force field, the aliphatic CH_n groups are treated as united atoms. Water was modeled using the simple point charge (SPC) model.[36]

2.1. Simulations of PNA in Solution. The simulations of PNA in solution were performed in a rectangular box using minimum image periodic boundary conditions. The bond lengths were constrained using the SHAKE algorithm[37] with a relative geometric tolerance of 10^{-4} allowing a time step of 2 fs. Electrostatic interactions were handled using a triple-range cutoff scheme[32] with cutoff radii of 0.8 nm (interactions updated every time step) and 1.4 nm (interactions updated every five time steps). The mean effect of omitted electrostatic interactions beyond the long-range cutoff distance of 1.4 nm was accounted for by including a reaction-field force using a dielectric permittivity of $\varepsilon_{rf} = 61$.[38] The weak coupling method[39] was used for keeping the temperature at 285 K and the pressure at 1 atm, using coupling times $\tau_T = 0.1$ ps, $\tau_p = 0.5$ ps and an isothermal compressibility of 4.575×10^{-4} $kJ^{-1}mol\ nm^3$. Solute and solvent were independently coupled to the heat bath. The initial structure of the PNA monomer or dimer was taken from the X-ray structure.[31] About 7000 water molecules were added in the computational box with initial edge lengths of 6 nm × 6 nm × 6 nm. Initial velocities were sampled from a Maxwell distribution at 60 K. The simulations were equilibrated for 100 ps. During this time interval, the temperature was raised from 60 to 285 K, and the harmonic positional restraints on the solute atoms were gradually released by reducing the force constant from 250 kJ mol^{-1} nm^{-2} to zero.

In the restrained simulations (MR, DR, PMR, and PDR; Table 1), in which the helical conformation of PNA as determined in the X-ray crystal structure was to be preserved, the tertiary nitrogen atoms in the PNA backbone were positionally restrained with a harmonic force constant of 250 kJ mol^{-1} nm^{-2}. As the position restrained simulations (MR, DR, PMR,

dx.doi.org/10.1021/ct400652w | J. Chem. Theory Comput. 2014, 10, 391−400

and PDR) do sample a restricted conformational space, they were run for only 10.5 ns, whereas the free unrestrained simulations (MF, DF, PMF, and PDF) were run for 25.5 ns.

2.2. Simulations of PNA in Crystal. The PNA hexamer crystallizes in space group P_1. The dimensions of the unit cell are a = 17.97 Å, b = 26.92 Å, c = 33.78 Å, and α = 88.19°, β = 79.41°, and γ = 82.51°. In order to obtain a sufficiently large computational box to use the GROMOS force-field nonbonded cutoff radius of 1.4 nm, the unit cell that contains a right-handed and a left-handed helix was copied 12 times, three times along the $\vec{a}$ and two times along the $\vec{b}$ and $\vec{a}$ axes, resulting in a triclinic simulation box which contains 24 PNA dimers. To reach the experimentally determined solvent content of 51.01%, 113 water molecules were added to each unit cell, which already contained 82 so-called crystallographic water molecules for which positions were present in the X-ray structure, resulting in 195 water molecules per unit cell and, therefore, 2340 water molecules per computational box.

Steepest-descent energy minimization (EM) of the configuration was performed applying periodic P_1 spatial boundary conditions, while positionally restraining the PNA atoms using a harmonic interaction with force constant 250 kJmol^{-1} nm^{-2}. For the equilibration of the system, the initial velocities were sampled from a Maxwell distribution at 50 K. During the equilibration MD simulation, the temperature was raised from 50 to 285 K, and the position restraining force constant was reduced from 250 kJmol^{-1} nm^{-2} to zero. The weak coupling method was used for keeping the temperature at 285 K with a coupling time τ_T = 0.1 ps. The crystal was then simulated for 10.5 ns. Solute and solvent were independently weakly coupled to a temperature bath at 285 K with a relaxation time of 0.1 ps. Bond lengths were constrained as in the solution simulations using a time step of 2 fs. The nonbonded interactions were handled as in the solution simulations.

2.3. Structural Analysis. In all simulations, the coordinate and energy trajectories were saved at 0.5 ps intervals, and structural analyses were performed using the entire trajectories. The atom positional root-mean-square deviations (RMSD) were calculated for bases, backbone, and all non-hydrogen PNA atoms after translational superposition of solute centers of mass and rotational least-squares fitting of atomic coordinates of heavy backbone atoms. Using the same superposition procedure, atom-positional root-mean-square fluctuations were calculated for all non-hydrogen PNA atoms. The hydrogen-bond analysis was performed every 10 ps on PNA dimers, and the criterion used in the hydrogen-bond analysis was 0.27 nm as the upper boundary for the H···A (A: acceptor) distance and 135° as the lower boundary of the D···H···A angle (D: donor). Only hydrogen bonds with occurrence larger than 5% were considered in the analyses.

2.4. Free Enthalpy Calculations. The free enthalpy change $\Delta G^{\text{pert ref}}$ upon perturbing force-field parameters in a simulation of a reference state (vertical lines, Figure 2) were calculated using the one-step perturbation method

$$\Delta G^{\text{pert ref}} = G^{\text{pert}} - G^{\text{ref}} = -k_B T \ln\langle e^{-(H_{\text{pert}}-H_{\text{ref}})/k_B T}\rangle_{\text{ref}} \quad (1)$$

where k_B is Boltzmann's constant, T is the temperature, H is the Hamiltonian of the reference or perturbed state, and $\langle ...\rangle_{\text{ref}}$ denotes an ensemble average over the trajectory generated using H_{ref}. The perturbed Hamiltonians represent changes in the following parameters: (i) partial charges of all atoms, of backbone atoms, or of nucleic acid base atoms changed by −10%, +5%, or +10% and (ii) force constants for all torsional angles in the nucleic acid building blocks raised by 10% or reduced by −10%. Block averaging[40] was used to calculate error estimates of the free enthalpy differences.

From the free enthalpy differences $\Delta G_{\text{D}}^{\text{pert ref}}$ and $\Delta G_{\text{M}}^{\text{pert ref}}$ calculated for a force-field perturbation on the dimer and monomer systems (cycles A in Figure 2), the effect of this force-field parameter change on the free enthalpy of PNA duplex formation using restrained (R) or unrestrained (F) PNA monomers and dimers can be obtained

$$\begin{aligned}\Delta G_{\text{DR MR}}^{\text{pert ref}} &= \Delta G_{\text{DR MR}}^{\text{pert}} - \Delta G_{\text{DR MR}}^{\text{ref}} \\ &= \Delta G_{\text{DR}}^{\text{pert ref}} - 2 \times \Delta G_{\text{MR}}^{\text{pert ref}}\end{aligned} \quad (2)$$

and

$$\begin{aligned}\Delta G_{\text{DF MF}}^{\text{pert ref}} &= \Delta G_{\text{DF MF}}^{\text{pert}} - \Delta G_{\text{DF MF}}^{\text{ref}} \\ &= \Delta G_{\text{DF}}^{\text{pert ref}} - 2 \times \Delta G_{\text{MF}}^{\text{pert ref}}\end{aligned} \quad (3)$$

The influence of the perturbation of force-field parameters on the free enthalpy of restraining a PNA monomer or dimer can be obtained from (cycles B in Figure 2)

$$\begin{aligned}\Delta G_{\text{DR DF}}^{\text{pert ref}} &= \Delta G_{\text{DR DF}}^{\text{pert}} - \Delta G_{\text{DR DF}}^{\text{ref}} \\ &= \Delta G_{\text{DR}}^{\text{pert ref}} - \Delta G_{\text{DF}}^{\text{pert ref}}\end{aligned} \quad (4)$$

or

$$\begin{aligned}\Delta G_{\text{MR MF}}^{\text{pert ref}} &= \Delta G_{\text{MR MF}}^{\text{pert}} - \Delta G_{\text{MR MF}}^{\text{ref}} \\ &= \Delta G_{\text{MR}}^{\text{pert ref}} - \Delta G_{\text{MF}}^{\text{pert ref}}\end{aligned} \quad (5)$$

The influence of the force-field perturbation on the change of environment from crystal to solution can be obtained by comparing $\Delta G_{\text{DC}}^{\text{pert ref}}$, the result for the simulation of the crystal divided by 24, and the number of PNA dimers in the crystal, with $\Delta G_{\text{DF}}^{\text{pert ref}}$ and $\Delta G_{\text{DR}}^{\text{pert ref}}$ (see thermodynamic cycles C in Figure 2)

$$\begin{aligned}\Delta G_{\text{DR DC}}^{\text{pert ref}} &= \Delta G_{\text{DR DC}}^{\text{pert}} - \Delta G_{\text{DR DC}}^{\text{ref}} \\ &= \Delta G_{\text{DR}}^{\text{pert ref}} - \Delta G_{\text{DC}}^{\text{pert ref}}\end{aligned} \quad (6)$$

$$\begin{aligned}\Delta G_{\text{DF DC}}^{\text{pert ref}} &= \Delta G_{\text{DF DC}}^{\text{pert}} - \Delta G_{\text{DF DC}}^{\text{ref}} \\ &= \Delta G_{\text{DF}}^{\text{pert ref}} - \Delta G_{\text{DC}}^{\text{pert ref}}\end{aligned} \quad (7)$$

The simulations PDF, PDR, PMF, and PMR (Table 1) allow for backward perturbations from the GROMOS 45A4 force field with 10% increased partial charges on the bases to the 45A4 force field itself.

3. RESULTS AND DISCUSSION

3.1. Structural Analysis. The atom-positional deviations of different sets of atoms of PNA from the initial X-ray structure presented in Figure 3 show that PNA dimers are stable in the crystal (Figure 3a–c) and in solution (Figure 3d). In general, the deviations for the base atoms (red) are bigger than for the backbone atoms (blue), but the differences are small. In the crystal simulation, the 24 PNA dimers show slightly different behavior, and as expected because of the choice of the X-ray structure as initial structure and the crystalline environment, most of them show smaller deviations than in solution. Not surprisingly, the unrestrained PNA monomer (Figure 3e) shows much bigger deviations from the crystal structure.

dx.doi.org/10.1021/ct400652w | J. Chem. Theory Comput. 2014, 10, 391−400

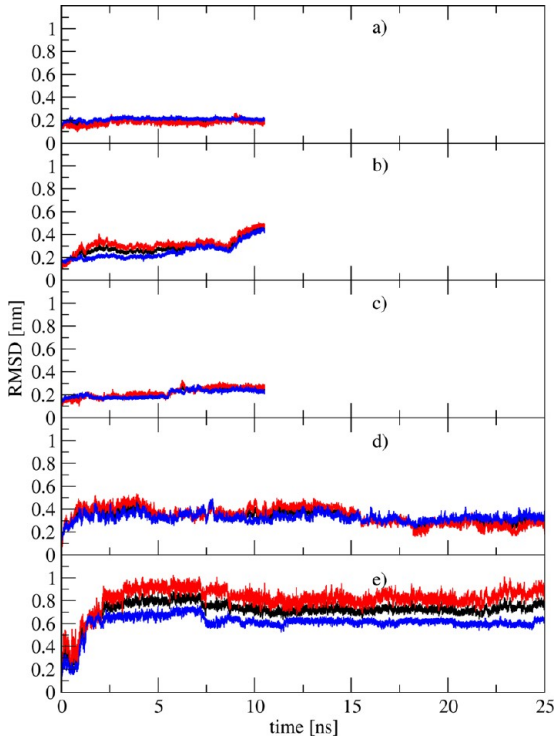

Figure 3. Atom-positional root-mean-square deviation of PNA from the initial X-ray structure in the different simulations (a–c) 2nd, 5th, and 18th PNA dimers in the crystal (DC), (d) unrestrained PNA dimer in solution (DF), and (e) unrestrained PNA monomer in solution (MF). Black: all heavy atoms. Red: all heavy base atoms. Blue: all heavy backbone atoms.

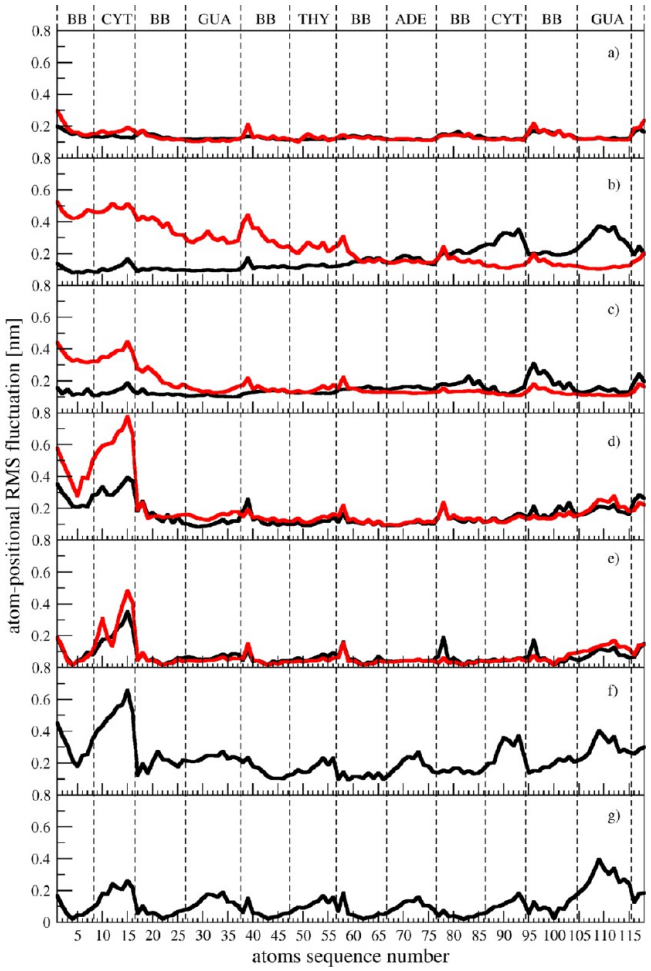

Figure 4. Atom-positional root-mean-square fluctuations for the different simulations. Black: first PNA strand of a dimer. Red: second PNA strand of a dimer. (a–c) 2nd, 5th, and 18th PNA dimer in the crystal. (d) Unrestrained and (e) restrained PNA dimer simulations, and (f) unrestrained and (g) restrained PNA monomer simulations.

The largest contribution to the RMSD values comes from the base pairs at the ends of the double helices, which is evident from the higher peaks in the atom-positional root-mean-squared fluctuations shown in Figure 4. It also illustrates that the 24 dimers of the crystal display different behavior. Panel a shows a PNA dimer in which the fluctuations are small for both strands of the helix, especially when compared with the PNA dimer shown in panel b. In the solution simulations (panels d and e), large fluctuations are evident for the first cytosine–guanine base pair. The fluctuation of this pair of nucleotides is similar to the fluctuation of these nucleotides in a single strand of the PNA dimer in solution (panel f). In general, the fluctuations are larger for the monomer than in the PNA dimer. Position restraining of the tertiary nitrogen atoms of the PNA backbone reduces the atom-positional fluctuations, while only slightly affecting the pattern as function of type of atom. Examples of PNA configurations for the unrestrained dimer simulations DF and PDF are shown in Figure 5 of the Supporting Information.

The hydrogen-bond analyses shown in Figures 5–Figure 11 are consistent with the overall behavior of the PNA molecules analyzed in terms of deviations from the crystal structure and atom-positional fluctuations.

The hydrogen-bond time series for three PNA dimers in the crystal (Figures 5–7) confirm that the PNA dimers in the crystal may behave differently from each other. The 2nd PNA dimer (Figure 5) is very stable. All Watson–Crick hydrogen bonds are present, and most of the time at least one hydrogen-bond between each base pair exists. In contrast, in the 5th PNA dimer (Figure 6), the hydrogen bonds in the middle of the double helix show a low occurrence, yet the helical structure is maintained. The 18th PNA dimer (Figure 7) shows yet another pattern of hydrogen bonding.

The simulations of a PNA dimer in solution show extensive Watson–Crick hydrogen bonding, except between the terminal base pairs. This corresponds to the large atom-positional fluctuations for atoms in these bases. As expected, position restraining of the tertiary nitrogen atoms of the PNA backbone increases the hydrogen bonding somewhat. Overall, the results of the structural analyses show that PNA dimers described by the GROMOS 45A4 force field are stable in solution as well in the crystal environment but may adopt locally different conformations. An example of the distribution of the hydrogen-bond distance and the hydrogen-bond angle for the hydrogen bond pair N1(8GUA)–O2(5CYT) in the unrestrained PNA dimer simulations DF and PDF is shown in Figure 6 of the Supporting Information.

3.2. One-Step Perturbation Free Enthalpy Estimates. In Tables 2 and 3, changes in free enthalpy $\Delta G^{\text{pert ref}}$ due to 11 perturbations of force-field parameters as obtained from five simulations (DC, DF, DR, MF, and MR) using the GROMOS 45A4 force field as the reference state are shown, together with the differences between these free enthalpy changes as defined in eqs 2–7. The $\Delta G^{\text{pert ref}}$ values (first 5 rows) show a nonlinear dependence upon a variation of atomic charges, which is not

dx.doi.org/10.1021/ct400652w | J. Chem. Theory Comput. 2014, 10, 391–400

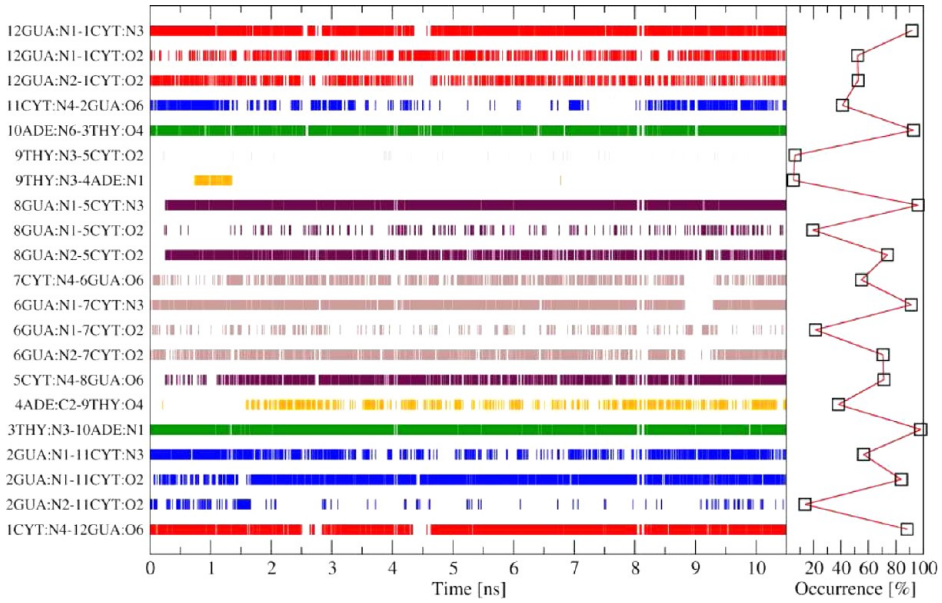

Figure 5. Time series of hydrogen bonds between the two strands of the 2nd PNA dimer with an occurrence higher than 5% in the crystal simulation. The first part of the label contains the donor residue number, name, and atom name, and the second part contains the acceptor atom. Red: hydrogen bonds between 1 CYT and 12 GUA. Blue: hydrogen bonds between 2 GUA and 11 CYT. Green: hydrogen bonds between 3 THY and 10 ADE. Orange: hydrogen bonds between 4 ADE and 9 THY. Maroon: hydrogen bonds between 5 CYT and 8 GUA. Brown: hydrogen bonds between 6 CYT and 7 GUA. Black: hydrogen bonds that include the backbone atoms. Gray: non-Watson−Crick hydrogen bonds.

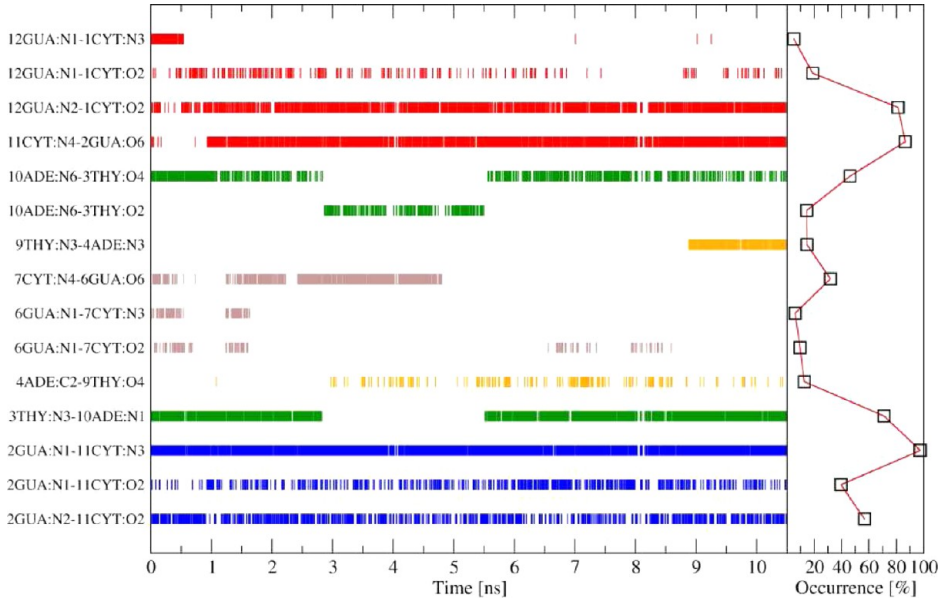

Figure 6. Time series of hydrogen bonds between the two strands of the 5th PNA dimer with an occurrence higher than 5% in the crystal simulation. The first part of the label contains the donor residue number, name, and atom name, and the second part contains the acceptor atom. Red: hydrogen bonds between 1 CYT and 12 GUA. Blue: hydrogen bonds between 2 GUA and 11 CYT. Green: hydrogen bonds between 3 THY and 10 ADE. Orange: hydrogen bonds between 4 ADE and 9 THY. Maroon: hydrogen bonds between 5 CYT and 8 GUA. Brown: hydrogen bonds between 6 CYT and 7 GUA. Black: hydrogen bonds that include the backbone atoms. Gray: non-Watson−Crick hydrogen bonds.

surprising considering the quadratic dependence of the electrostatic potential energy upon the atomic charges. The dependence of $\Delta G^{\text{pert ref}}$ upon the torsional-angle energy force constant is rather linear with a maximum difference of 1.3 kJ mol^{-1} between the ±10% variations of the torsional-angle force constant.

3.2.1. Free Enthalpy of PNA Dimer Formation. In rows 6 and 7 of Tables 2 and 3, estimates of the effect of force-field parameter variations upon the free enthalpy of PNA dimer formation, $\Delta G^{\text{pert ref}}_{\text{DR MR}}$ (eq 2) obtained from the restrained simulations, and $\Delta G^{\text{pert ref}}_{\text{DR MF}}$ (eq 3) obtained from the unrestrained simulations are shown. In the restrained case, increasing all charges destabilizes the dimer, i.e., $\Delta G^{\text{pert ref}}_{\text{DR MR}} > 0$, in the unrestrained case the opposite effect is observed. So, positionally restraining some backbone atoms significantly influences the results of this perturbation. Increasing only the base charges clearly disfavors dimer formation, as the nucleobases get more hydrophilic, whereas increasing the backbone charges favors dimer formation.

dx.doi.org/10.1021/ct400652w | J. Chem. Theory Comput. 2014, 10, 391−400

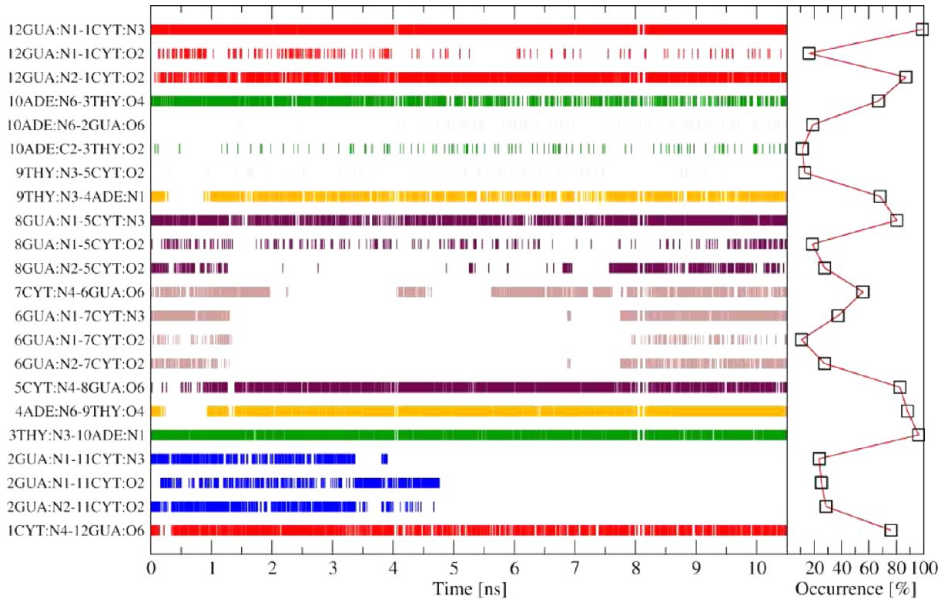

Figure 7. Time series of hydrogen bonds between the two strands of the 18th PNA dimer with an occurrence higher than 5% in the crystal simulation. The first part of the label contains the donor residue number, name, and atom name, and the second part contains the acceptor atom. Red: hydrogen bonds between 1 CYT and 12 GUA. Blue: hydrogen bonds between 2 GUA and 11 CYT. Green: hydrogen bonds between 3 THY and 10 ADE. Orange: hydrogen bonds between 4 ADE and 9 THY. Maroon: hydrogen bonds between 5 CYT and 8 GUA. Brown: hydrogen bonds between 6 CYT and 7 GUA. Black: hydrogen bonds that include the backbone atoms. Gray: non-Watson−Crick hydrogen bonds.

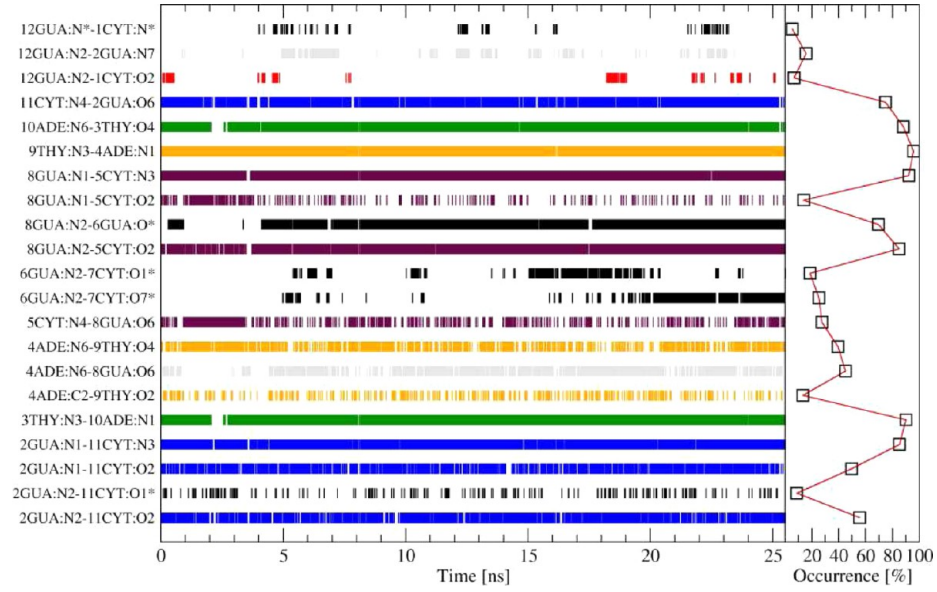

Figure 8. Time series for all hydrogen bonds with an occurrence higher than 5% in the DF simulation. The first part of the label contains the donor residue number, name, and atom name, and the second part contans the acceptor atom. Red: hydrogen bonds between 1 CYT and 12 GUA. Blue: hydrogen bonds between 2 GUA and 11 CYT. Green: hydrogen bonds between 3 THY and 10 ADE. Orange: hydrogen bonds between 4 ADE and 9 THY. Maroon: hydrogen bonds between 5 CYT and 8 GUA. Brown: hydrogen bonds between 6 CYT and 7 GUA. Black: hydrogen bonds that include the backbone atoms. Gray: non-Watson−Crick hydrogen bonds.

3.2.2. Free Enthalpy of Backbone Position Restraining. Rows 8 and 9 of Tables 2 and 3 show estimates of the effect of force-field parameter variations upon the free enthalpy change of introducing position restraints for some backbone atoms, $\Delta G^{\text{pert ref}}_{\text{DR DF}}$ (eq 4) obtained from the simulations of the dimer in solution, and $\Delta G^{\text{pert ref}}_{\text{MR MF}}$ (eq 5) obtained from the simulations of the monomer in solution. For the dimer, the values range from −0.8 to +2.2 kJ mol^{-1}, while a larger range, −3.0 to +3.5 kJ mol^{-1}, is found for the monomer because its helical conformation is not maintained by the other strand as in the dimer.

3.2.3. Free Enthalpy of Crystal Dissolution. Rows 10 and 11 of Tables 2 and 3 contain estimates of the effect of force-field parameter variations upon the free enthalpy of dissolution of the crystal, $\Delta G^{\text{pert ref}}_{\text{DR DC}}$ (eq 6) obtained from simulations of the dimer restrained in solution, and $\Delta G^{\text{pert ref}}_{\text{DF DC}}$ (eq 7) obtained from simulations of the dimer unrestrained in solution and in the crystal. Increasing all charges stabilizes the crystal, mainly due to the base charges, while increasing the backbone charges destabilizes the crystal dimer with respect to the dimer in solution. Position restraining has only a minor influence.

dx.doi.org/10.1021/ct400652w | J. Chem. Theory Comput. 2014, 10, 391−400

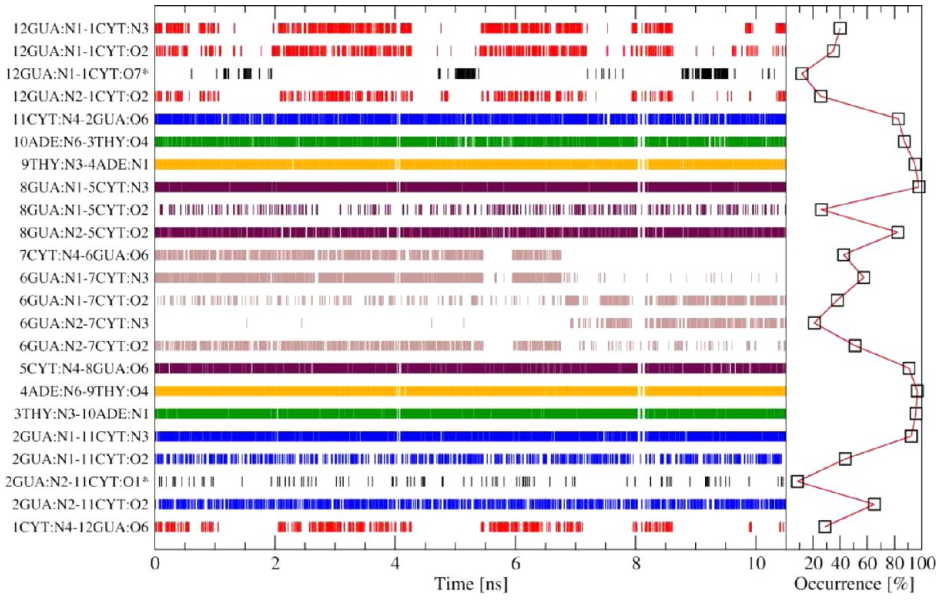

Figure 9. Time series for all hydrogen bonds with an occurrence higher than 5% in the DR simulation. The first part of the label contains the donor residue number, name, and atom name, and the second part contains the acceptor atom. Red: hydrogen bonds between 1 CYT and 12 GUA. Blue: hydrogen bonds between 2 GUA and 11 CYT. Green: hydrogen bonds between 3 THY and 10 ADE. Orange: hydrogen bonds between 4 ADE and 9 THY. Maroon: hydrogen bonds between 5 CYT and 8 GUA. Brown: hydrogen bonds between 6 CYT and 7 GUA. Black: hydrogen bonds that include the backbone atoms. Gray: non-Watson–Crick hydrogen bonds.

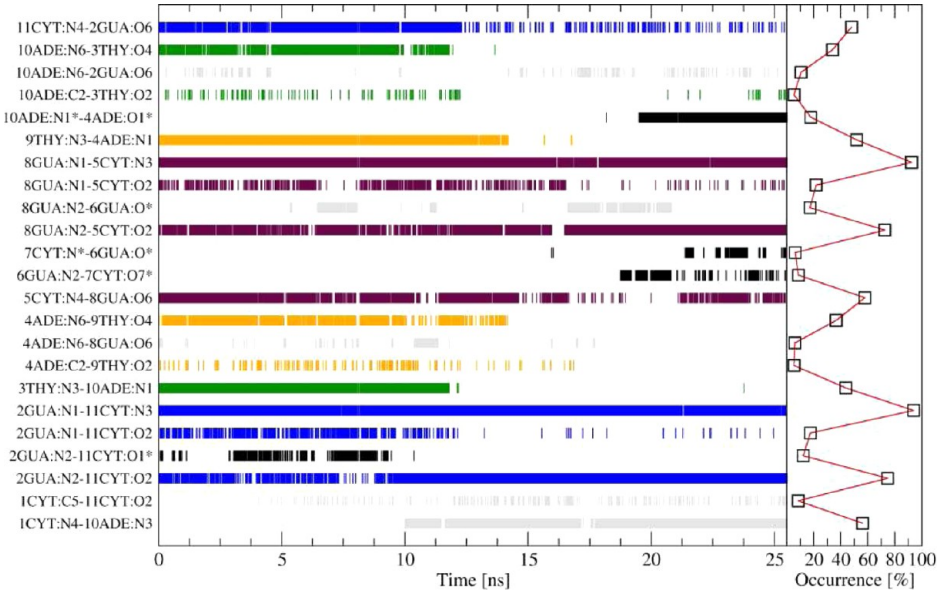

Figure 10. Time series for all hydrogen bonds with an occurrence higher than 5% in the PDF simulation. The first part of the label contains the donor residue number, name, and atom name, and the second part contains the acceptor atom. Red: hydrogen-bonds between 1 CYT and 12 GUA. Blue: hydrogen bonds between 2 GUA and 11 CYT. Green: hydrogen bonds between 3 THY and 10 ADE. Orange: hydrogen bonds between 4 ADE and 9 THY. Maroon: hydrogen bonds between 5 CYT and 8 GUA. Brown: hydrogen bonds between 6 CYT and 7 GUA. Black: hydrogen bonds that include the backbone atoms. Gray: non-Watson–Crick hydrogen bonds.

Although increasing the charges makes the nucleotide more hydrophilic, its destabilizing effect on dimer formation is minor due to the low water content of the crystal.

3.3. Accuracy Estimation by Backward Perturbation. The ΔG values obtained from one-step perturbation are well converged, as illustrated in Figure 7 of the Supporting Information. However, whether one-step perturbation, eq 1, yields correct free enthalpy differences $\Delta G^{\text{pert ref}}$ depends on the degree of overlap between the configurational ensembles of H^{ref} and H^{pert}.[22,30] A test of the reliability of one-step perturbation values $\Delta G^{\text{pert ref}}$ is to perform simulations for H^{pert} and then use eq 1 to obtain $\Delta G^{\text{ref pert}}$ from so-called backward perturbation.

To validate the one-step perturbation results for variations of the GROMOS force-field 45A4 discussed above, simulations based on 45A4 with 10% increased base charges were performed for the unrestrained and restrained dimer and monomer in solution (Table 1). Increasing the base charges by 10% is one of the largest changes in the force-field parameters that were considered and should therefore provide an estimation of the upper bound of the inaccuracy.

dx.doi.org/10.1021/ct400652w | J. Chem. Theory Comput. 2014, 10, 391–400

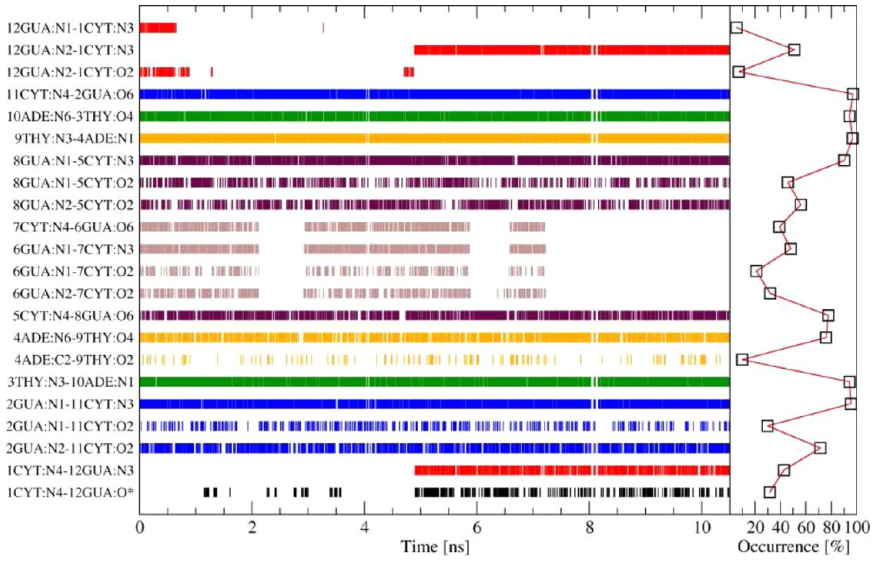

Figure 11. Time series for all hydrogen bonds with an occurrence higher than 5% in the PDR simulation. The first part of the label is the donor residue and hydrogen donor atom, and the second part is the acceptor residue and acceptor atom. The star marks an atom in the backbone of these residue. Red: hydrogen bonds between 1 CYT and 12 GUA. Blue: hydrogen bonds between 2 GUA and 11 CYT. Green: hydrogen bonds between 3 THY and 10 ADE. Orange: hydrogen bonds between 4 ADE and 9 THY. Maroon: hydrogen bonds between 5 CYT and 8 GUA. Brown: hydrogen bonds between 6 CYT and 7 GUA. Black: hydrogen bonds that include the backbone atom. Gray: non-Watson−Crick hydrogen bonds.

Table 2. Free Enthalpy Differences in kJ mol^{-1} for Perturbing All or Only Base Charges in PNA by About ±10% and 5% from the 45A4 Force-Field Charges

perturbation	all charge +10%	all charge +5%	all charge −10%	base charge +10%	base charge +5%	base charge −10%
$\Delta G_{DC}^{pert\ ref}$	−391.9 ± 0.4	−192.7 ± 0.3	358.0 ± 0.3	−269.7 ± 0.4	−132.0 ± 0.3	240.5 ± 0.4
$\Delta G_{DF}^{pert\ ref}$	−389.5 ± 0.3	−188.6 ± 0.1	338.0 ± 0.7	−264.3 ± 0.4	−126.9 ± 0.1	223.0 ± 0.3
$\Delta G_{DR}^{pert\ ref}$	−388.6 ± 0.6	−188.1 ± 0.1	339.2 ± 0.4	−262.1 ± 0.3	−126.1 ± 0.1	222.3 ± 0.4
$\Delta G_{MF}^{pert\ ref}$	−193.1 ± 0.5	−93.2 ± 0.1	167.1 ± 0.2	−132.9 ± 0.3	−63.7 ± 0.1	112.2 ± 0.2
$\Delta G_{MR}^{pert\ ref}$	−196.0 ± 0.3	−94.9 ± 0.1	170.5 ± 0.3	−133.4 ± 0.3	−64.1 ± 0.1	112.9 ± 0.2
$\Delta G_{DR\ MR}^{pert\ ref}$	3.4 ± 0.8	1.6 ± 0.2	−1.9 ± 0.7	4.6 ± 0.6	2.0 ± 0.2	−3.5 ± 0.6
$\Delta G_{DF\ MF}^{pert\ ref}$	−3.2 ± 1.0	−2.3 ± 0.2	3.8 ± 0.8	1.4 ± 0.7	0.5 ± 0.2	−1.4 ± 0.5
$\Delta G_{DR\ DF}^{pert\ ref}$	0.9 ± 0.6	0.5 ± 0.2	1.2 ± 0.8	2.2 ± 0.5	0.8 ± 0.2	−0.7 ± 0.5
$\Delta G_{MR\ MF}^{pert\ ref}$	−2.9 ± 0.6	−1.7 ± 0.1	3.5 ± 0.4	−0.5 ± 0.4	−0.4 ± 0.1	0.7 ± 0.3
$\Delta G_{DR\ DC}^{pert\ ref}$	3.3 ± 0.7	4.6 ± 0.3	−18.8 ± 0.5	+7.6 ± 0.5	+5.9 ± 0.3	−18.2 ± 0.6
$\Delta G_{DF\ DC}^{pert\ ref}$	2.4 ± 0.5	4.1 ± 0.3	−20.0 ± 0.8	+5.4 ± 0.6	+5.1 ± 0.3	−17.5 ± 0.6

Table 3. Free Enthalpy Differences in kJ mol^{-1} for Perturbing All Backbone (bb) PNA Charges, by ±10% and 5% and for Perturbing the Force Constant of the Torsional-Angle Energy Term by ±10% from the 45A4 Force-Field Values

perturbation	bb charge +10%	bb charge +5%	bb charge −10%	torsion +10%	torsion −10%
$\Delta G_{DC}^{pert\ ref}$	−127.9 ± 0.5	−62.3 ± 0.3	112.4 ± 0.3	17.0 ± 0.4	−18.3 ± 0.2
$\Delta G_{DF}^{pert\ ref}$	−131.0 ± 0.2	−62.9 ± 0.1	110.7 ± 0.2	15.7 ± 0.1	−16.9 ± 0.1
$\Delta G_{DR}^{pert\ ref}$	−131.4 ± 0.1	−63.2 ± 0.1	111.0 ± 0.2	16.4 ± 0.1	−17.7 ± 0.1
$\Delta G_{MF}^{pert\ ref}$	−62.4 ± 0.3	−30.0 ± 0.1	52.6 ± 0.1	7.8 ± 0.1	−8.4 ± 0.1
$\Delta G_{MR}^{pert\ ref}$	−65.4 ± 0.1	−31.4 ± 0.1	55.1 ± 0.1	8.8 ± 0.1	−9.5 ± 0.1
$\Delta G_{DR\ MR}^{pert\ ref}$	−0.5 ± 0.3	−0.4 ± 0.1	0.8 ± 0.3	−1.2 ± 0.2	1.3 ± 0.2
$\Delta G_{DF\ MF}^{pert\ ref}$	−6.1 ± 0.5	−3.0 ± 0.2	5.5 ± 0.3	0.0 ± 0.2	0.0 ± 0.2
$\Delta G_{DR\ DF}^{pert\ ref}$	−0.4 ± 0.2	−0.3 ± 0.1	0.3 ± 0.3	0.7 ± 0.2	−0.8 ± 0.2
$\Delta G_{MR\ MF}^{pert\ ref}$	−3.0 ± 0.3	−1.5 ± 0.1	2.5 ± 0.2	1.9 ± 0.1	−1.1 ± 0.1
$\Delta G_{DR\ DC}^{pert\ ref}$	−3.5 ± 0.5	−0.9 ± 0.3	−1.4 ± 0.4	−0.7 ± 0.4	0.6 ± 0.2
$\Delta G_{DF\ DC}^{pert\ ref}$	−3.1 ± 0.5	−0.7 ± 0.3	−1.7 ± 0.4	−1.4 ± 0.4	1.4 ± 0.2

The hydrogen-bond analyses of the PNA dimer simulations with the perturbed force-field are presented in Figures 10 and 11. The comparison with the corresponding simulations done with the original force field (Figures 8 and 9) shows in general lower Watson−Crick hydrogen-bond occurrences. Especially for the unrestrained simulations (Figures 8 and 10), 10% increased base charges cause destabilization of the dimer. The same trend can be seen to lesser extent in the restrained simulations. Yet, the helical structure is still preserved.

The results from the forward and backward one-step perturbations using the 45A4 ensemble and the ensemble generated with 10% increased base charges are shown in Figures

12 and 13 in the form of the thermodynamic cycle involving dimer formation (cycle A in Figure 2) and the one involving the introduction of backbone position restraints (cycle B in Figure 2), respectively. The forward (down) and backward (up) $\Delta G^{\text{pert ref}}$ values differ by less than 0.1 kJ mol^{-1} for the restrained monomer and less than 0.8 kJ mol^{-1} for the restrained dimer (Figure 12). The values for the unrestrained monomer and dimer are 0.2 kJ mol^{-1} and 2.0 kJ mol^{-1}, respectively. These rather small deviations lead to close estimates of $\Delta G^{\text{pert ref}}_{\text{DR MR}}$ and $\Delta G^{\text{pert ref}}_{\text{DF MF}}$ using both ensembles; the differences lie within the accuracy estimates.

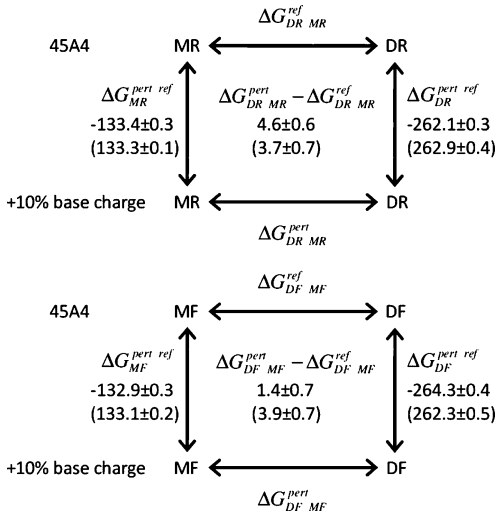

Figure 12. Thermodynamic cycles involving a force-field perturbation and dimer formation (cycles A in Figure 2) with the forward and backward (between parentheses) results of a force-field change involving 10% increased base charges. Upper graph: position restrained simulations. Lower graph: unrestrained simulations.

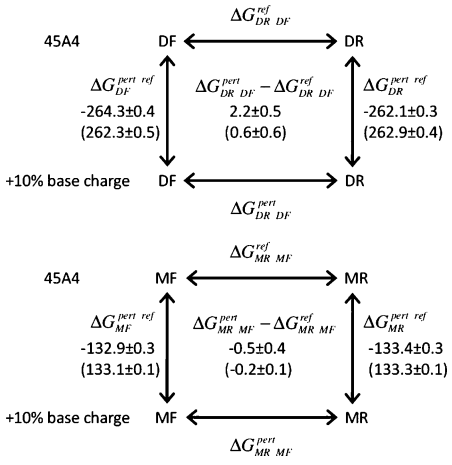

Figure 13. Thermodynamic cycles involving a force-field perturbation and restraining atom positions (cycles B in Figure 2) with the forward and backward (between parentheses) results of a force-field change involving 10% increased base charges. Upper graph: dimer simulations. Lower graph: monomer simulations.

4. CONCLUSION

The effect of a variation of base or backbone atomic charges or the force constant of the torsional-angle term in the force field used to simulate PNA monomers and dimers in solution or in the crystal upon the free enthalpy of formation in solution, $\Delta G^{\text{pert ref}}_{\text{DR MR}}$ and $\Delta G^{\text{pert ref}}_{\text{DR MF}}$, and upon dissolution of the crystal, $\Delta G^{\text{pert ref}}_{\text{DR DC}}$ and $\Delta G^{\text{pert ref}}_{\text{DR DC}}$, has been investigated using the technique of one-step perturbation. A variation of the torsional-angle force constant by ±10% induced linear changes in $\Delta G^{\text{pert ref}}$ values. Counterintuitively, it was found that dimer formation in solution is favored by a decrease in base charges and an increase in backbone charges of PNA from the GROMOS 45A4 force-field values. This can be explained by the increase in hydrophilicity of the nucleobases upon an increase in partial charges. The crystal form of the PNA dimer is stabilized with respect to the dimer in solution by an increase in the base charges, while variation of the backbone charges has a small influence due to the low water content of the crystal. So, increasing the base charges disfavores dimer formation in solution, while it favors crystallization of a dimer. This result illustrates the complexity of the relation between relative free enthalpy of a system and a change in force-field parameters. Using one-step perturbation, such relationships can be efficiently elucidated. In the present case of the GROMOS 45A4 force field, no need of improvement by a change of force-field parameters was indicated.

■ ASSOCIATED CONTENT

Ⓢ Supporting Information

Atomic numbering schemes used in the GROMOS force-field parameter tables for PNA adenine, guanine, thymine, and cytosine (Figures 1−4). Atom names, masses, GROMOS integer atom codes describing the Lennard−Jones parameters, and partial charges for PNA adenine, guanine, thymine, and cytosine (Tables 1, 6, 11, and 16). GROMOS bond types for adenine, guanine, thymine, and cytosine (Tables 2, 7, 12, and 17). GROMOS bond-angle types for adenine, guanine, thymine, and cytosine (Tables 3, 8, 13, and 18). GROMOS dihedral-angle types for adenine, guanine, thymine. and cytosine (Tables 4, 9, 14, and 19). GROMOS improper dihedral-angle types for adenine, guanine, thymine, and cytosine (Tables 5, 10, 15, and 20). PNA conformations from unrestrained simulations DF and PDF (Figure 5). N1−O2 distance distributions and N1−H1−O2 bond-angle distributions for the hydrogen bond 8GUA:N1−5CYT:O2 for the unrestrained simulations DF and PDF (Figure 6). Time series of $\Delta G^{\text{pert ref}}_{\text{DF}}$ for perturbing base charges in PNA by 10% (Figure 7). This material is available free of charge via the Internet at http://pubs.acs.org.

■ AUTHOR INFORMATION

Corresponding Author

*E-mail: dolenc@chem.ethz.ch.

Present Address

‖Interfaculty Institute of Biochemistry, University of Tübingen, Auf der Morgenstelle 15, 72076 Tübingen, Germany.

Notes

The authors declare no competing financial interest.

■ ACKNOWLEDGMENTS

This work was financially supported by the National Center of Competence in Research (NCCR) in Structural Biology, Grant 200020-137827 of the Swiss National Science Foundation, and Grant 228076 of the European Research Council, which is gratefully acknowledged. J.D. acknowledges financial support from the Slovenian Research Agency (ARRS) under Grant P1-0201.

REFERENCES

(1) Cheatham, T. E.; Young, M. A. *Biopolymers* **2000**, *56*, 232−256.
(2) Cheatham, T. E. I. *Curr. Opin Struct. Biol.* **2004**, *14*, 360−367.
(3) Orozco, M.; Noy, A.; Pérez, A. *Curr. Opin. Struct. Biol.* **2008**, *18*, 185−193.
(4) Pérez, A.; Luque, F. J.; Orozco, M. *Acc. Chem. Res.* **2012**, *45*, 196−205.
(5) Kastenholz, M. A.; Hünenberger, P. H. *J. Phys. Chem. B* **2004**, *108*, 774−788.
(6) Kräutler, V.; Hünenberger, P. H. *Mol. Simul.* **2008**, *34*, 491−499.
(7) Anderson, C. F.; Record, M. T. *Annu. Rev. Phys. Chem.* **1995**, *46*, 657−700.
(8) Denisov, V. P.; Halle, B. *Proc. Natl. Acad. Sci. U.S.A.* **2000**, *97*, 629−633.
(9) Auffinger, P.; Hashem, Y. *Curr. Opin. Struct. Biol.* **2007**, *17*, 325−333.
(10) Nielsen, P. E.; Haaima, G. *Chem. Soc. Rev.* **1997**, *26*, 73−78.
(11) Nielsen, P. E.; Egholm, M.; Buchardt, O. *Bioconjugate Chem.* **1994**, *5*, 3−7.
(12) Nielsen, P. *Perspect. Drug Discovery Des.* **1996**, *4*, 76−84.
(13) Nielsen, P. E.; Egholm, M.; Berg, R. H.; Buchardt, O. *Science* **1991**, *254*, 1497−1500.
(14) Watson, J. D.; Crick, F. H. *Nature* **1953**, *171*, 737−738.
(15) Stafforst, T.; Hilvert, D. *Angew. Chem., Int. Ed.* **2010**, *49*, 9998−10001.
(16) He, W.; Hatcher, E.; Balaeff, A.; Beratan, D. N.; Gil, R. R.; Madrid, M.; Achim, C. *J. Am. Chem. Soc.* **2008**, *130*, 13264−13273.
(17) Datta, B.; Bier, M. E.; Roy, S.; Armitage, B. A. *J. Am. Chem. Soc.* **2005**, *127*, 4199−4207.
(18) Soliva, R.; Sherer, E.; Luque, F. J.; Laughton, C. A.; Orozco, M. *J. Am. Chem. Soc.* **2000**, *122*, 5997−6008.
(19) Sen, S.; Nilsson, L. *J. Am. Chem. Soc.* **2001**, *123*, 7414−7422.
(20) Sen, S.; Nilsson, L. *J. Am. Chem. Soc.* **1998**, *120*, 619−631.
(21) Egholm, M.; Buchardt, O.; Christensen, L.; Behrens, C.; Freier, S. M.; Driver, D. A.; Berg, R. H.; Kim, S. K.; Norden, B.; Nielsen, P. E. *Nature* **1993**, *365*, 566−568.
(22) Liu, H.; Mark, A. E.; van Gunsteren, W. F. *J. Phys. Chem.* **1996**, *100*, 9485−9494.
(23) Schäfer, H.; van Gunsteren, W. F.; Mark, A. E. *J. Comput. Chem.* **1999**, *20*, 1604−1617.
(24) Pitera, J. W.; van Gunsteren, W. F. *J. Phys. Chem. B* **2001**, *105*, 11264−11274.
(25) Lin, Z.; van Gunsteren, W. F.; Liu, H. *J. Comput. Chem.* **2011**, *32*, 2290−2297.
(26) Lin, Z.; Kornfeld, J.; Mächler, M.; van Gunsteren, W. F. *J. Am. Chem. Soc.* **2010**, *132*, 7276−7278.
(27) Oostenbrink, C. *J. Comput. Chem.* **2009**, *30*, 212−221.
(28) de Ruiter, A.; Oostenbrink, C. *J. Chem. Theory Comput.* **2012**, *8*, 3686−3695.
(29) Lin, Z.; van Gunsteren, W. F. *Mol. Phys.* **2013**, *111*, 2126−2130.
(30) Lin, Z.; Liu, H.; van Gunsteren, W. F. *J. Comput. Chem.* **2010**, *31*, 2419−2427.
(31) Rasmussen, H.; Kastrup, J. S.; Nielsen, J. N.; Nielsen, J. M.; Nielsen, P. E. *Nat. Struct. Biol.* **1997**, *4*, 98−101.
(32) van Gunsteren, W. F.; Billeter, S.; Eising, A.; Hünenberger, P.; Krüger, P.; Mark, A.; Scott, W.; Tironi, I. *Biomolecular Simulation: The GROMOS96 Manual and User Guide*; Vdf Hochschulverlag AG an der ETH Zürich: Zürich, Switzerland, 1996.
(33) Christen, M.; Hünenberger, P. H.; Bakowies, D.; Baron, R.; Bürgi, R.; Geerke, D. P.; Heinz, T. N.; Kastenholz, M. A.; Kräutler, V.; Oostenbrink, C.; Peter, C.; Trzesniak, D.; van Gunsteren, W. F. *J. Comput. Chem.* **2005**, *26*, 1719−1751.
(34) Soares, T. A.; Hünenberger, P. H.; Kastenholz, M. A.; Kräutler, V.; Lenz, T.; Lins, R. D.; Oostenbrink, C.; van Gunsteren, W. F. *J. Comp, Chem.* **2005**, *26*, 725−737.
(35) Oostenbrink, C.; Villa, A.; Mark, A. E.; van Gunsteren, W. F. *J. Comput. Chem.* **2004**, *25*, 1656−1676.
(36) Berendsen, H. J. C.; Postma, J. P. M.; van Gunsteren, W. F.; Hermans, J. Intermolecular Forces. In *Molecular Liquids - Dynamics and Interaction*; Reidel: Dordrecht, The Netherlands, 1981; pp 331−342.
(37) Ryckaert, J.-P.; Ciccotti, G.; Berendsen, H. J. C. *J. Comput. Phys.* **1977**, *23*, 327−341.
(38) Tironi, I. G.; Sperb, R.; Smith, P. E.; van Gunsteren, W. F. *J. Chem. Phys.* **1995**, *102*, 5451−5459.
(39) Berendsen, H. J. C.; Postma, J. P. M.; van Gunsteren, W. F.; DiNola, A.; Haak, J. R. *J. Chem. Phys.* **1984**, *81*, 3684−3690.
(40) Allen, M. P.; Tildesley, D. J. *Computer Simulation of Liquids*; Clarendon Press: Oxford, 2006.